



Melanocortin receptor 4 as a new target in melanoma therapy: Anticancer activity of the inhibitor ML00253764 alone and in association with *B-raf* inhibitor vemurafenib

Paola Orlandi^a, Marta Banchi^a, Francesca Vaglini^b, Marco Carli^b, Stefano Aringhieri^{b,1}, Arianna Bandini^a, Carla Pardini^b, Cristina Viaggi^b, Michele Lai^b, Greta Ali^c, Alessandra Ottani^d, Eleonora Vandini^d, Patrizia Guidi^a, Margherita Bernardeschi^{a,2}, Veronica La Rocca^{b,e}, Giulio Francia^f, Gabriella Fontanini^c, Mauro Pistello^b, Giada Frenzilli^a, Daniela Giuliani^d, Marco Scarselli^b, Guido Bocci^{a,*}

^a Dipartimento di Medicina Clinica e Sperimentale, Università di Pisa, Pisa, Italy

^b Dipartimento di Ricerca Traslationale e delle Nuove Tecnologie in Medicina e Chirurgia, Università di Pisa, Pisa, Italy

^c Dipartimento di Patologia Chirurgica, Medica, Molecolare e dell'Area Critica, Università di Pisa, Pisa, Italy

^d Dipartimento di Scienze Biomediche, Metaboliche e Neuroscienze, Sezione di Farmacologia e Medicina Molecolare, Università di Modena e Reggio Emilia, Modena, Italy

^e Scuola Superiore Sant'Anna, Pisa, Italy

^f Border Biomedical Research Center, University of Texas at El Paso (UTEP), El Paso, TX, USA

ARTICLE INFO

Keywords:

MC4R
Melanoma
ML00253764
Vemurafenib
Synergism
Apoptosis
In vitro model
In vivo model

ABSTRACT

The aim of our study is to investigate *in vitro* and *in vivo* MC4R as a novel target in melanoma using the selective antagonist ML00253764 (ML) alone and in combination with vemurafenib, a *B-raf*V600E inhibitor.

The human melanoma *B-raf* mutated A-2058 and WM 266-4 cell lines were used. An MC4R null A-2058 cell line was generated using a CRISPR/Cas9 system. MC4R protein expression was analysed by western blotting, immunohistochemistry, and immunofluorescence. Proliferation and apoptotic assays were performed with ML00253764, whereas the synergism with vemurafenib was evaluated by the combination index (CI) and Loewe methods. ERK1/2 phosphorylation and BCL-XL expression were quantified by western blot. *In vivo* experiments were performed in Athymic Nude-Foxn1^{nu} male mice, injecting subcutaneously melanoma cells, and treating animals with ML, vemurafenib and their concomitant combination. Comet and cytome assays were performed.

Our results show that human melanoma cell lines A-2058 and WM 266-4, and melanoma human tissue, express functional MC4R receptors on their surface. MC4R receptors on melanoma cells can be inhibited by the selective antagonist ML, causing antiproliferative and proapoptotic activity through the inhibition of phosphorylation of ERK1/2 and a reduction of BCL-XL. The concomitant combination of vemurafenib and ML caused

Abbreviations: α -MSH, α -melanocyte stimulating hormone; ACTH, adrenocorticotrophic hormone; AgRP, Agouti-Related Peptide; Akt, protein kinase B; ANOVA, analysis of variance; BCL-2, B-cell lymphoma 2; BCL-XL, B-cell lymphoma-extra large; B-raf, v-raf murine sarcoma viral oncogene homolog B1; cAMP, cyclic adenosine monophosphate; CDS, coding sequence; CI, combination index; CRISPR/Cas9, clustered regularly interspaced short palindromic repeats/CRISPR-associated protein 9; DMEM, Dulbecco's Modified Eagle's Medium; DMSO, dimethyl sulfoxide; EDTA, ethylenediaminetetraacetic acid; EMEM, Eagle's Minimum Essential Medium; ERK1/2, Extracellular signal-regulated kinase 1/2; Fa, Fraction affected; FBS, fetal bovine serum; GB, glioblastoma; HCl, hydrogen chloride; HO-1, heme oxygenase-1; HRP, horseradish peroxidase; IgG, immunoglobulin G; IHC, immunohistochemistry; MANOVA, multifactor analysis of variance; MAPK, mitogen-activated protein kinase; MC1R, melanocortin receptor 1; MC4R, melanocortin receptor 4; MI, mitotic index; ML, ML00253764; MMC, Mitomycin C; MRT, multiple range test; NaCl, sodium chloride; NPB, nucleoplasmic bridges; p.o., *per os*; PAGE, polyacrylamide gel electrophoresis; PBS, phosphate buffered saline; PCR, polymerase chain reaction; pSTAT SER, phospho signal transducer and activator of transcription serine; PVDF, polyvinylidene fluoride; RIPA, radioimmunoprecipitation assay; RNP, Ribonucleoproteins; rpm, revolutions per minute; s.c., subcutaneous; SD, standard deviation; SDS, sodium dodecyl sulfate; SEM, standard error of the mean; SphK1, sphingosine kinase 1; TO-PRO3, trimethyl-[3-[4-[(E,3Z)-3-(3-methyl-1,3-benzothiazol-2-ylidene)prop-1-enyl]quinolin-1-ium-1-yl]propyl]azanium.

* Correspondence author.

E-mail address: guido.bocci@unipi.it (G. Bocci).

¹ Present address: Dipartimento Salute Mentale e Dipendenze Patologiche Forlì -Cesena, Ausl Romagna, Italy.

² Present address: Istituto Italiano di Tecnologia, Pontedera, Italy.

<https://doi.org/10.1016/j.bcp.2023.115952>

Received 9 September 2023; Accepted 27 November 2023

Available online 29 November 2023

0006-2952/© 2023 The Author(s). Published by Elsevier Inc. This is an open access article under the CC BY license (<http://creativecommons.org/licenses/by/4.0/>).

a synergistic effect on melanoma cells *in vitro* and inhibited *in vivo* tumor growth in a preclinical model, without causing mouse weight loss or genotoxicity.

Our original research contributes to the landscape of pharmacological treatments for melanoma, providing MC4R antagonists as drugs that can be added to established therapies.

1. Introduction

Melanocortin peptides are derived from the polypeptide proopiomelanocortin, α -melanocyte stimulating hormone (α -MSH) and adrenocorticotrophic hormone (ACTH). They have been implicated in pigment regulation, secretion of adrenocortical hormones, energy homeostasis, and neuroprotective activity, and they act *via* the interaction with five different melanocortin receptors [1,2]. The melanocortin receptor 4 (MC4R) is expressed in various human cells such as skin melanocytes, astrocytes, and neural progenitor cells [3]. MC4R expression in the hypothalamic arcuate nucleus is highly involved in food intake regulation, and reports suggest it also has a role in inflammation, neuroprotection, and astrocyte functions [4,5].

MC4R is a G protein-coupled receptor and its intracellular signaling pathway involves the stimulation of adenylyl cyclase with an increased synthesis of cyclic adenosine monophosphate (cAMP), involving also mitogen-activated protein kinase (MAPK) extracellular signal-regulated kinase 1/2 (ERK-1/2) activation [6]. Caruso and colleagues [7] reported that α -MSH protects astrocytes from apoptosis through MC4R stimulation by decreasing caspase-3 activity. A recent article reported the *in vitro* preventing effect of cell death and the increasing cell proliferation after ACTH binding to MC4R, expressed in oligodendroglia and oligodendroglia precursor cells [8]. Interestingly, it has been also described a basal (constitutive) activity in wild type and mutant MC4R in the absence of agonists [9], and the presence of an endogenous competitive antagonist called Agouti-Related Peptide (AgRP) [10]. Indeed, human AgRP operates as an inverse agonist for the human MC4R, suppressing the constitutive activity of the receptor both in transfected B16/G4F mouse melanoma cells and in membrane preparations [10].

Currently, there are no data available on functional MC4R expression or activity in human melanoma cells. Nonetheless, Vaglini and colleagues recently showed that human glioblastoma (GB) cell lines and tissues express MC4R receptors [11] and that their inhibition with the non-peptide, selective MC4R inhibitor ML00253764 (ML) [12] caused antiproliferative and pro-apoptotic effects as a result of inhibition of ERK1/2 and protein kinase B (Akt) phosphorylation [11]. Additionally, an association of temozolomide and the MC4R antagonist caused highly synergic activity *in vitro* and *in vivo* in a GB murine model, indicating the possibility with this combination of a dose reduction in the chemotherapeutic drug and, thus, reducing the relative toxicity of this regimen whilst retaining its therapeutic effect [11].

These premises and data may indicate a direct effect of the selective MC4R selective antagonist ML – a drug originally designed to prevent cachexia - on tumors derived from cells that normally express functional MC4Rs such as melanomas. Given the inhibition of GB tumor cells *in vitro* and *in vivo*, we hypothesize that the functional inhibition of MC4R by ML could directly arrest proliferation and induce apoptosis of melanoma cells, which would greatly enhance the therapeutic effect of available target therapies in patients affected by these aggressive tumors, thus representing a completely novel treatment. Therefore, the aim of our study is to investigate *in vitro* and *in vivo* MC4R as a novel target in melanoma using a selective antagonist alone and in combination with vemurafenib, a *v-raf murine sarcoma viral oncogene homolog B1* (*B-raf*) V600E inhibitor [13].

2. Materials and methods

2.1. Cell lines and drugs

The human melanoma *B-raf* V600E mutated A-2058 (ATCC-CRL-11147), *B-raf* V600D mutated WM 266-4 (ECACC-91061233) cell lines were cultured in Dulbecco's Modified Eagle's Medium (DMEM) and Eagle's Minimum Essential Medium (EMEM), respectively. The passage number of cell lines were authenticated by the vendors. The media were added with heat-inactivated fetal bovine serum (FBS) at 10 %, 1 % Sodium Pyruvate, 1 % L-glutamine, and 100 U/mL penicillin, 100 mg/mL streptomycin. Cells were maintained at 37 °C in 5 % CO₂ with a humidity at 95 %. Reagents for cell line cultures were purchased from Sigma Chemical Co. (St Louis, MO, USA). Sterile cell culture plastics were obtained from Sarstedt (Nümbrecht, Germany). Vemurafenib was from Selleckchem (Houston, TX, USA), and it was solubilized in dimethyl sulfoxide (DMSO). The small molecule ML (chemical name: 2-[2-[2-(5-Bromo-2-methoxyphenyl)ethyl]-3-fluorophenyl]-4,5-dihydro-2-1H-imidazole hydrochloride) was obtained from Tocris Bioscience (Bristol, UK), and it was prepared in sterile water.

To perform *in vitro* experiments, a 10 mM stock solution was prepared for both drugs. Dimethyl sulfoxide (DMSO) concentration in the control's media was the one utilized to dilute the highest concentration of vemurafenib in the medium of treated samples for the same experiment.

2.2. Clustered regularly interspaced short palindromic repeats/CRISPR-associated protein 9 (CRISPR/Cas9) design, transfection, and transduction

The CRISPR/Cas9 system was used to eliminate the *MC4R* gene in the A-2058 cell line. CRISPR/Cas9 editing of *MC4R* gene was designed using the human *MC4R* coding sequence (NG_016441). The chosen gRNAs were selected to minimize the off-target activity, according to the Benchling algorithm:

gRNA1: 5'-GCCUUUUCCAAGGGACUCACGUUUUAGAGCUAUGCU-3';

gRNA2: 5'-UGGUGAACUCCACCCACCGUGUUUAGAGCUAUGCU-3'.

gRNAs were synthesised by IDT (Integrated DNA Technology, Iowa, USA). Ribonucleoproteins (RNP) were assembled following manufacturer's protocol (Integrated DNA Technology, Iowa, USA). RNP transfection of A-2058 cells was performed using NEON Nucleofector system (Thermo Scientific, Massachusetts, USA) using 10 μ l transfection kit with the following specifications: 1600 V, 10 ms, 3 pulses. 48 h later, 5x10³ cells were serially diluted in 96-well plates. Single cell-derived clones were then analysed by polymerase chain reaction (PCR), followed by sequencing analysis. PCR screening were performed on total genomic DNA extraction using the following primer pairs: FWD: GTGAAACTCTGTGCATCCGT REV: AACTCCATGTCAAGCTCTGG. To fully characterize the mutation induced by gene-editing and separate the two alleles during sequencing, we sub-cloned the PCR products into pJet 1.2 vector, following manufacturer's instruction (CloneJet, Thermo Scientific, Massachusetts, USA). Off-target activity was measured in A-2058 cells using Surveyor Nuclease Assay (IDT, Coralville, Iowa, USA) following the manufacturer's protocol. No off-target activity was found for both A-2058 C1 and A-2058 C7 clones (data not shown). A schematic representation of CRISPR/Cas9 gene ablation strategy used to inactivate the *MC4R* gene in A-2058 Clones 1 and 7 is shown in Fig. 1. The

sequencing analysis of Clones 1 and 7 revealed large deletions in both alleles and the introduction of early stop codons by gene-editing of MC4R.

2.3. Immunohistochemistry, immunofluorescence and western blotting of MC4R in melanoma cells

To evaluate the levels of MC4R protein expression in melanoma cells, we studied A-2058, A-2058 Clone 1 (MC4R null) and WM 266–4 cells. This experimental procedure has previously been described by us [11]. Thus, in brief, cells (2×10^4) were seeded on glass coverslips that had been placed in 12-well plates. Cultured cells were fixed 72 h later in a solution of 4 % paraformaldehyde (made up in phosphate buffered saline, PBS), and then blocked with 15 % normal goat serum and 0.2 % Triton X-100. The cells were incubated with 20 $\mu\text{g}/\text{ml}$ of a rabbit anti-MC4R antibody overnight (GTX31382; Gene Tex International Corporation; Irvine, CA, USA). Slides were washed three times with PBS. Next, the slides were incubated with biotinylated anti-rabbit immunoglobulin G (IgG) (Vector Laboratories; Burlingame, CA, USA), and thereafter with avidin–biotin conjugated to peroxidase (Vector Laboratories). We omitted the primary antibody in some slides as a negative control to assess background staining. The stained cells were imaged using a Nikon inverted microscope at $\times 20$ magnification. Next, micrographs were generated using a Nikon D40x digital camera. For the immunofluorescent studies, cells were fixed onto slides and then incubated with a 1:250 dilution (in PBS) of secondary goat anti-rabbit fluorescent antibody (Alexa Fluor 488; Abcam; Cambridge, MA, USA). Cells were stained with trimethyl-[3-[4-[(E,3Z)-3-(3-methyl-1,3-benzothiazol-2-ylidene)prop-1-enyl]quinolin-1-ium-1-yl]propyl]azanium;diiodide (TO-PRO3; Molecular Probes; Eugene, OR, USA) diluted 1:1000 (in PBS) for nuclear staining, and coverslips were visualized using a confocal Leica TCS SP5 laser-scanning microscope. We used both $\times 40$ and $\times 60$ magnification. We used cells with no primary antibody treatment as a negative control.

Western blotting analysis was performed as previously described [11]. Briefly, radioimmunoprecipitation assay (RIPA) buffer was added

to cell pellets. Cells were first sonicated, and then centrifuged (14,000 \times g for 15 min in a cold centrifuge), and protein concentration in the lysates was evaluated by using Bradford's reagent. Forty μg of total proteins lysate for each sample were first denatured by boiling in reducing buffer, and then isolated by electrophoresis. Lysates were then transferred onto polyvinylidene fluoride (PVDF) membranes. The membranes were exposed to MC4R primary antibody (dilution 1:500, ab75506; Abcam) for 12 h at 4 °C. The membranes were then exposed to a secondary antibody peroxidase-conjugated (Cell Signaling Technology; Danvers, MA, USA) followed by conjugate detection. For loading controls, the blots were also probed for β -tubulin expression (antibody from Cell Signaling Technology).

2.4. Immunofluorescence of MC4R and MC1R in human tissue

A Melanoma specimen was from the archival samples of the University of Pisa collection. The human specimen was obtained by qualified pathologists within routine diagnostic aims, and this was following a protocol that was approved by the Ethic Committee of the University of Pisa. As previously described [11], the tissue block was first fixed in buffered formalin. It was subsequently washed in PBS, and then processed for paraffin embedding. Sections were cut with a microtome (at 10 μm thickness). The slides were then deparaffinized, rehydrated, and then processed for hematoxylin/eosin staining, and for immunofluorescence studies. To evaluate the expression of MC4R and melanocortin receptor 1 (MC1R) proteins, the tissue slides were first washed in PBS. They were then incubated for 30 min in blocking solution (which consisted of 15 % normal goat serum and 0.2 % Triton X-100 in PBS). The tissue samples were incubated overnight at 4 °C with a mouse anti-MC1R antibody (ab230675, Abcam) used at a working concentration of 10 $\mu\text{l}/\text{ml}$ in PBS and a rabbit anti-MC4R antibody (GTX31382) at 2.5 $\mu\text{l}/\text{ml}$ in PBS. Tissue slides were then incubated for 90 min with a secondary goat anti-mouse red fluorescent antibody (Alexa Fluor 647) as well as an anti-rabbit green, fluorescent antibody (Alexa Fluor 488); and both these secondary antibodies were diluted 1:250 in PBS. The slides

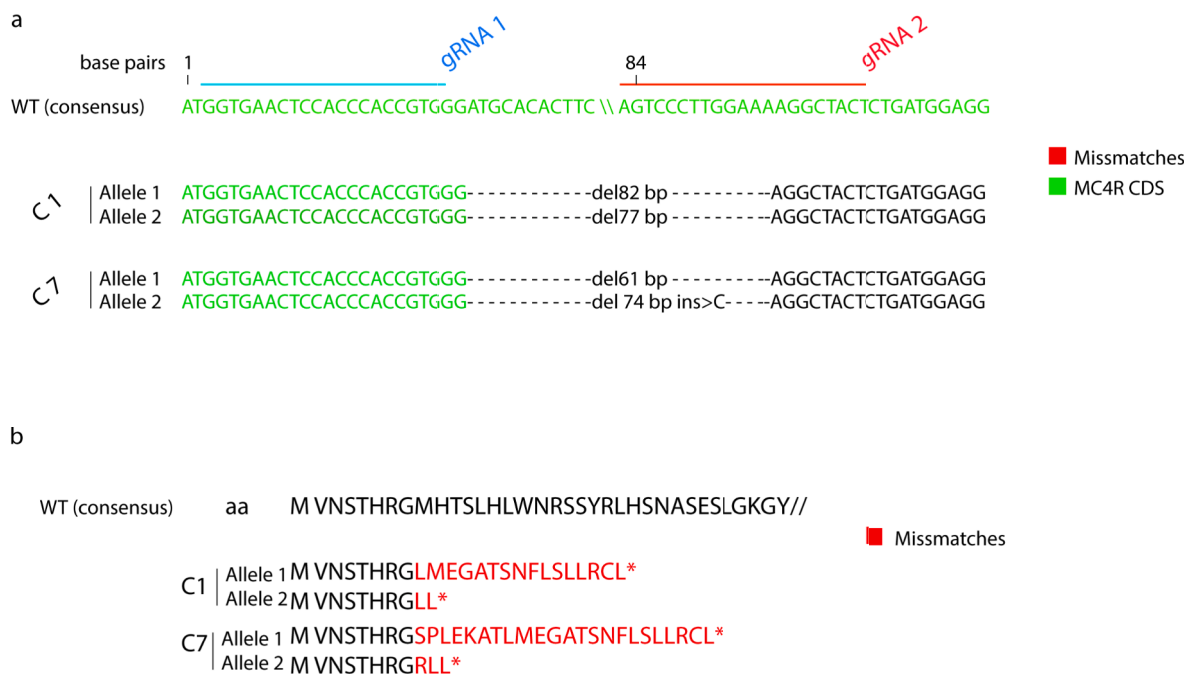


Fig. 1. **a**) Schematic representation of CRISPR/Cas9 gene ablation strategy used to inactivate the MC4R gene. Green letters indicate conserved coding sequence (CDS). Sequencing analysis of Clones 1 and 7 revealed large deletions in both alleles. **b**) Protein sequence prediction based on the sequencing analysis shown in a. The analysis revealed the introduction of early stop codons by gene-editing of MC4R. (For interpretation of the references to color in this figure legend, the reader is referred to the web version of this article.)

were then washed three times, and nuclear staining was performed by using 10 μ l of Dapi/Antifade solution (Sigma-Aldrich, St Louis, MO, USA). The tissue slides were mounted and visualized under a Leica TCS SP5 confocal laser-scanning microscope used at \times 60 magnification (Leica Microsystems, Mannheim, Germany).

2.5. Antiproliferative and apoptosis assays

In vitro antiproliferative activity was tested in WM 266–4, A-2058 and A-2058 Clone 1 melanoma cell lines. The experimental procedures have been previously described [11] with some modifications. Briefly, cancer cells were seeded in 24-well sterile plastic plates and treated with ML (0.001–50 μ M) and vemurafenib (0.001–100 μ M) continuously for 72 h, adding fresh solutions with new medium every 24 h. Controls were exposed to their respective vehicles. Viable cells (evaluated by trypan blue dye exclusion) were counted with a hemocytometer. The data are reported as the percentage of the vehicle-treated cells. All experiments were reiterated, separately, three times with at least three samples for each drug concentration. The drug concentration that caused a 50% reduction of cell proliferation (IC_{50}) vs. vehicle-treated samples was estimated by non-linear regression fit of the mean values of nine samples for each drug concentration.

The activity of the combined treatment of ML and vemurafenib were evaluated on both WM 266–4 and A-2058 melanoma cells with the concomitant program of an established molar concentration ratio of 1:1, including ML (0.01–50 μ M) plus vemurafenib (0.01–50 μ M) for 72 h. To estimate the possible synergistic activity between ML and vemurafenib, the combination index (CI) method [14] and the Loewe additivity model [15] were followed. In brief, synergism, or antagonism for ML and vemurafenib was assessed based on a multiple drug-effect equation, and quantified by the CI, where $CI < 1$, $CI = 1$, and $CI > 1$ mean synergism, additive effect, and antagonism, respectively. The CI indexes were calculated with the CalcuSyn v.2.0 software (Biosoft, Cambridge, UK). The synergistic, additive, and antagonistic effects of the combined drugs were measured and graphically summarized using the Loewe additivity model, with the Combeneft software (v.2.021).

To quantify apoptosis induced by ML treatments, WM 266–4 and A-2058 3×10^5 cells were seeded in 100-mm sterile dishes and tested for 72 h with ML, vemurafenib and their concomitant combination, at their respective IC_{50} s, and with vehicle alone. At the completion of the treatment period, cells were collected, and the samples were analyzed with the Cell Death Detection enzyme-linked immunosorbent assay (ELISA) Plus kit (Roche, Switzerland) [16]. The data were expressed as percentages versus the mean value of vehicle-treated absorbance (obtained from at least nine samples) that was set at 100 %. All experiments were reiterated, separately, three times with at least three samples for drug concentration. Moreover, to obtain images of the apoptotic cells, 2×10^4 melanoma cells were seeded on coverslips in a 12-well plate and tested with ML for 72 h at their IC_{50} s. At the completion of the treatment time, the coverslips were washed with PBS, and the cells were fixed, and stained with TO-PRO3. The cells were finally observed under a Leica TCS SP5 confocal laser-scanning microscope.

To identify the proteins involved in the proliferative and apoptotic process the western blotting on heme oxygenase-1 (HO-1), phospho signal transducer and activator of transcription serine (pSTAT SER) and B-cell lymphoma-extra large (BCL-XL) protein was performed on WM 266–4 and A-2058 cells treated with ML at their experimental IC_{50} s with the same protocol procedure described above. The primary antibodies for HO-1, pSTAT SER and BCL-XL were obtained from Cell Signaling Technology and the membranes were also tested for β -tubulin protein adopting an anti- β -tubulin antibody.

2.6. Extracellular signal-regulated kinase (ERK) 1/2 and phospho (P)-ERK1/2 western blotting

A-2058 and A-2058 Clone 1 melanoma cells were starved overnight and treated with ML (0.1–10,000 nM), or vehicle alone in serum free medium for 30 min or at 1,000 nM at different time points (from 1 to 60 min). After treatment, cells were lysed with a lysis buffer including Tris-hydrogen chloride (HCl) pH 8.0, sodium chloride (NaCl), ethylenediaminetetraacetic acid (EDTA), Triton, sodium dodecyl sulfate (SDS) and protease inhibitor mix. Whole-cells lysates were centrifuged at 12000 rpm for 15 min at 4 °C to obtain supernatants. Protein concentration in the samples was measured using Bradford procedure. Proteins were separated by SDS-polyacrylamide gel electrophoresis (PAGE) and transferred to a PVDF membrane. Membranes were blocked in 5 % nonfat milk for 1 h at a temperature of 25 °C, washed and incubated overnight at 4 °C with anti-ERK-P M9692 (pERK-1/2 44 kDa and 42 kDa, Thr183 and Tyr185; 1:1,000; Sigma-Aldrich). Bound primary antibodies were detected with secondary antibody horseradish peroxidase (HRP) conjugated A4416 (1:20,000; Sigma-Aldrich) for ERK-P incubated for 1 h at room temperature. The detection of bands was performed with Luminata Forte Western HRP Substrate (Millipore, Darmstadt, Germany) on a Kodak Image Station 440 CF. The same PVDFs were stripped in acidic solution (pH 2.0) and re-blocked in 5 % nonfat milk for 1 h. After stripping, membranes were incubated overnight with anti-ERK-Total M5670 (1:40,000; Sigma-Aldrich) at 4 °C and 1 h with anti-rabbit HRP conjugated SAB3700852 (1:2,000; Sigma-Aldrich) at room temperature and bands were detected as described above. The bands quantification was performed with Kodak 1D image analysis software.

2.7. In vivo experiments

Athymic Nude-Foxn1^{nu} male mice (20–25 g) were obtained by Envigo (Milan, Italy) and they had access to sterile food and water. All animal procedures and housing were done in agreement with the approval of the Academic Organization Responsible for Animal Welfare (OPBA, Organismo Preposto per il Benessere Animale) of the University of Pisa and of the Italian Ministry of Health (authorization number 191/2019-PR).

The previously published *in vivo* experimental procedure [17] was followed with minor modifications. Briefly, $3 \times 10^6 \pm 5$ % viable A-2058 and WM 266–4 in 0.2 ml serum-free medium were injected subcutaneously (s.c.) in each mouse between the scapulae. Mouse weights were checked, and tumor extents were assessed every 2–3 days in two crosswise lines using a caliper. The tumor volume (mm^3) was measured as $[(w1 \times w2 \times w2) \times (\pi/6)]$, where $w1$ and $w2$ were the largest and the smallest mass widths (mm), respectively [18]. The mice were assigned randomly to different groups of treatments, including six animals *per* group. After the onset of an established tumor (about 50 mm^3), the mice were treated with ML 30 mg/kg s.c. daily [11], vemurafenib 75 or 100 mg/kg *per os* (p.o.) every other day [19] and their concomitant combination.

At the completion of the experimental time, mice were euthanized by an anesthetic overdose and tumor tissues were fixed in formalin and then embedded in paraffin for MC4R and MC1R immunofluorescence, as described above, and for immunohistochemistry as previously reported [17]. Tumor slices (5 μ m thick) were stained with haematoxylin and eosin and were evaluated for the necrosis index (% of necrotic area), the mitotic index (MI). Immunohistochemistry (IHC) for CD31 (clone JC70, Ventana Medical System) and active caspase-3 (ab2302, Abcam, Cambridge, UK) was assessed in an independent way by two different pathologists. Negative controls were carried out by excluding the primary antibodies.

2.8. Comet and Cytome assays

A-2058, A-2058 Clone-1 and WM 266-4 cells lines were exposed ML (0–1,000 nM) for 48 h. As a positive control for the Comet assay, we used Hydrogen peroxide (100 μ M for 10 min treatment). Similarly, as positive control for the Cytome assay, we used Mitomycin C (MMC) at a concentration of 0.1 μ g/ml.

2.8.1. Comet assay

DNA damage evaluation in melanoma cells was essentially carried out as previously reported [20,21]. Briefly, melanoma cell suspensions were embedded in low melting agarose (0,5%). Next the cells were spread onto microscope slides that had been pretreated with regular melting agarose (1 %). These slides were subsequently dipped into a lysis solution, in which they were incubated at 4 °C for 1 h to completely lyse the cells membranes. The slides were then placed by immersion into an alkali solution for approximately 20 min. The slides were then electrophoresed for 20 min. At this stage, the slides were adjusted to neural pH with Tris–HCl. They were then stained with ethidium bromide, and were then observed under a microscope (at 400 \times magnification). For each of the experiments conducted, we assessed the percentage of DNA that migrated in the direction of the anode (noted as % tail DNA), and these results were quantified with an image analyzer (Kinetic Imaging Ltd, Komet, Version 5). We measured at least 25 random nuclei for each slide, and we also scored two slides for each of the different treatments. Next the mean values were calculated. These experiments were conducted in dimmed light to prevent artificial DNA damage.

2.8.2. Cytome assay

Melanoma cells were treated for 48 h. Cytochalasin B (6 mg/ml) (Sigma Aldrich) was added at 44 h after seeding. The treated cells were washed, detached, and then collected by centrifugation (1,800 rpm for 10 min) 72 h after seeding. Next, the cell pellets were incubated with 1 ml of hypotonic solution at 37 °C and thereafter with 80 μ l of freshly prepared pre-fixative solution (methanol and acetic acid at 3:5). The cells were then centrifuged at 1,800 rpm for 10 min. Cell pellets were resuspended in a freshly made ice-cold fixative solution (composed of methanol and acetic acid at 7:1) and kept at + 4 °C for at least half an hour. After a second fixative step, the cells were placed onto microscope slides and subsequently stained with 4 % Giemsa. We used two slides for each treatment and 2,000 binucleated cells with observably well-preserved cytoplasm were scored under a light microscope to determine and count the frequency of nucleoplasmic bridges (NPB) as described [22].

2.9. Statistical analysis

For the data analysis, investigators were blinded to which samples/animals represented treatments and controls. The data (mean \pm SD or SEM) underwent to analysis of variance (ANOVA), followed by the Student–Newman–Keuls test. The level of significance was established at $P < 0.05$. Analyses were carried out with the GraphPad Prism software package version 7.0 (GraphPad Software, Inc., San Diego, CA). For the *in vivo* experiments, 6 animals were used per group in order to give 80 % power to oneway ANOVA analysis, against a difference in tumor volumes equal or greater than 0.50*sd, with a nominal alpha error rate = 0.05. The power calculation was carried out using G*Power 3 software. For the Comet and Cytome assays, we performed Multifactor Analysis of Variance (MANOVA) taking into consideration dose, experimental time, culture, and the experiment, as factors. The multiple range test (MRT) was used to detect statistically significant differences ($P < 0.05$) among the different experimental groups. For the analysis, we used the statistical software SGWIN (Windows 98).

3. Results

3.1. MC4R is expressed in human melanoma cell lines and in tissue samples

The immunohistochemistry and the immunofluorescence of melanoma A-2058 and WM 266–4 cells showed the existence of MC4R protein on A-2058 (Fig. 2A and C, respectively) and WM 266–4 (Fig. 2E and G, respectively) cells in comparison to negative controls where the primary antibody anti-MC4R was omitted (Fig. 2B and D and Fig. 2F and H). Western blotting validated the expression of the melanocortin receptor 4 in both A-2058 and WM 266–4 cell lines (Fig. 2I) with the presence of two marked bands, as previously described in glioblastoma cells [11]. The human patient melanoma tissue sample, shown in Fig. 2J, exhibited a robust MC4R immunoreactivity (green color) (Fig. 2K). Moreover, the immunofluorescence of melanoma slices incubated with both MC4R (green color) and MC1R (red color) antibody (Fig. 2L) showed an intense staining for MC4R but only few positive MC1R cells.

3.2. ML inhibits melanoma cell proliferation alone and in combination with vemurafenib

No statistical differences were noted between the proliferation rate (Fig. 3A) and the pERK/ERK ratio (Fig. 3B) of A-2058 and A-2058 Clone 1 (the MC4R null cell line) melanoma cells. The antiproliferative effects of ML on WM 266–4, A-2058 and A-2058 Clone 1 melanoma cells treated for 72 h showed a concentration-dependent pharmacological activity. The calculated IC₅₀s were found to be 33.7 nM, 11.1 nM, and 360.1 nM, respectively (Fig. 4A). Vemurafenib showed concentration/response curves with a strong antiproliferative activity on A-2058 cells (IC₅₀ = 1.1 nM) and WM 266–4 (IC₅₀ = 7.3 nM) melanoma cells treated for 72 h (Fig. 4B). The concomitant treatment of ML and vemurafenib for 72 h caused a highly synergistic antiproliferative effect on both the melanoma cell lines A-2058 (Fig. 4C) and WM 266–4 (Fig. 4D) with the CI values far below 1, obtaining an amplified antiproliferative effect compared to what expected by the simple sum of the effects if administered individually. The calculation - with the Loewe additivity model - of the drug combination effects, mapped as a three-dimensional synergy diagram, demonstrated that the association of ML with vemurafenib in A-2058 cells was strongly synergic (Fig. 4E). The Loewe method corroborated the findings also for WM 266–4 cells (Fig. 4F) at all the percentage of cell proliferation inhibition.

3.3. Decrease of ERK1/2 phosphorylation by ML in melanoma cells

Western blot analysis demonstrated that a 30-min exposure of ML inhibited in a concentration-dependent manner the quantity of the active pERK1/2 in A-2058 cells (Fig. 5A), and the ratio of pERK/ERK protein bands of ML-exposed cells emerged significantly declined already at low nanomolar concentrations ($P < 0.05$; Fig. 5B). The absence of MC4R in A-2058 Clone 1 cells abolished the concentration-dependent effects of ML (Fig. 5A), with a significant difference ($P < 0.05$; Fig. 5B) compared to the A-2058 cells harboring MC4R on their plasma membrane. Moreover, the inhibition of the phosphorylated form of ERK1/2 was also time-dependent with a marked effect (more than 50 %) after 30-, 45- and 60-min ML exposure in A-2058 but not in the A-2058 Clone 1 cells (Fig. 5C). The image analysis of the blots confirmed the statistical inhibition of the phosphorylation of ERK1/2 by ML in A-2058 cells ($P < 0.05$; Fig. 5D) and the absence of this activity on Clone 1 cells (Fig. 5D).

3.4. Induction of apoptosis in melanoma cells by ML

This apoptotic process was quantified using an ELISA test. Fig. 6A shows a significant increase in the extent of DNA fragmentation at 10 nM of ML (the antiproliferative IC₅₀) after 72 h of treatment in A-2058 cells

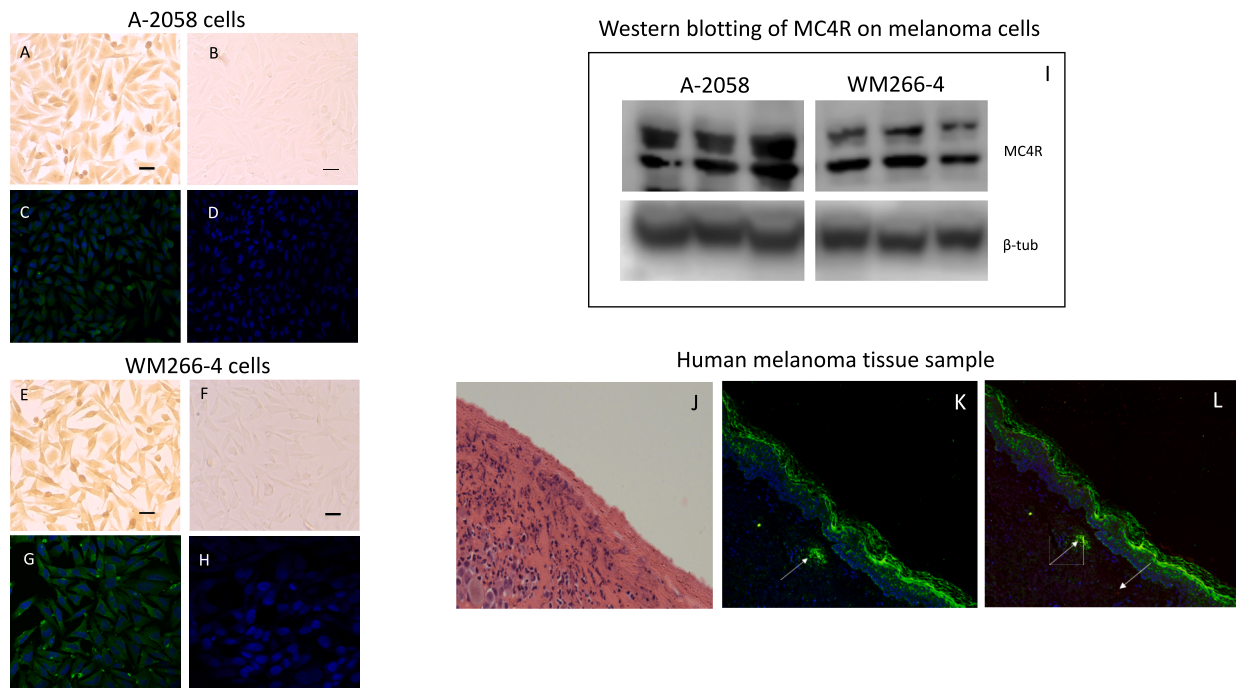


Fig. 2. Immunohistochemistry (A and B) and immunofluorescence (C and D) of A-2058 cells (upper microscopic pictures) stained with melanocortin receptor-4 (MC4R) antibody (left microscopic pictures) and negative control (right microscopic pictures), performed by omission of the primary antibody. Immunohistochemistry (E and F) and immunofluorescence (G and H) of WM 266–4 cells (lower microscopic pictures) stained with MC4R antibody (left microscopic pictures) and negative control (right microscopic pictures). Scale bar, 25 μ m. Immunoblotting (I) of MC4R protein and of housekeeping gene product β -tubulin from a triplicate of cellular lysates of melanoma A-2058 and WM 266–4 cell lines. MC4R and melanocortin receptor-1 (MC1R) immunoreactivity in a human tissue sample of cutaneous melanoma. Hematoxylin and eosin (J) stained section of melanoma sample and immunofluorescence of MC4R (K; color green) alone, and MC4R with MC1R (L; color red). Magnification of the images: J x 20; K and L x 40. (For interpretation of the references to color in this figure legend, the reader is referred to the web version of this article.)

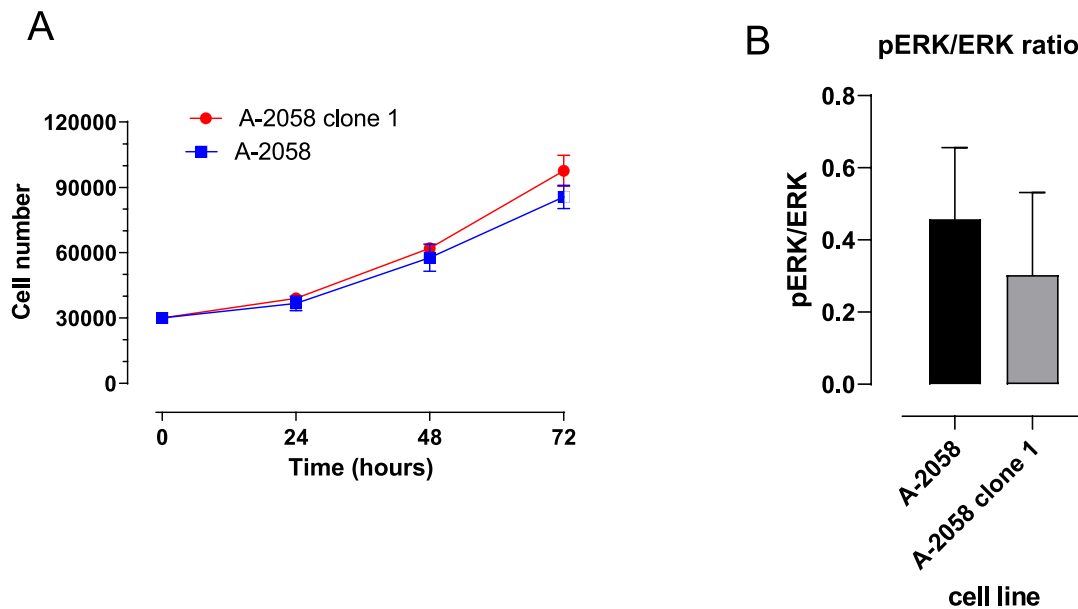


Fig. 3. Proliferation rate (A) and pERK/ERK ratio (B) of A-2058 (MC4R WT) and A-2058 Clone 1 (MC4R null) were reported. No statistical differences were found between the two cell lines for both the studied characteristics. The data are presented as mean (\pm SEM) values of cell numbers; columns and bars represent mean values \pm SD of image analysis quantification of pERK/ERK ratio of A-2058 and A-2058 clone 1 cell lines.

compared to vehicle-treated cells, and also the 35 nM concentration (the antiproliferative IC_{50}) significantly enhanced the apoptosis in WM 266–4 cells after 72 h (Fig. 6A). Moreover, the combination treatment of ML and vemurafenib (at their respective IC_{50} s) markedly intensified the apoptotic process in both the cell lines if compared to the single

treatments (Fig. 6A). TO-PRO3 iodide incubation revealed at confocal microscope a weak fluorescence of normal nuclei (Fig. 6B) of A-2058 vehicle-treated cells (i.e., non-apoptotic cells); instead, the 10 nM of ML-treated sample showed an enhanced fluorescence of shrunken nuclei (Fig. 6C) that are characteristic of apoptotic cells. After exposure to 10

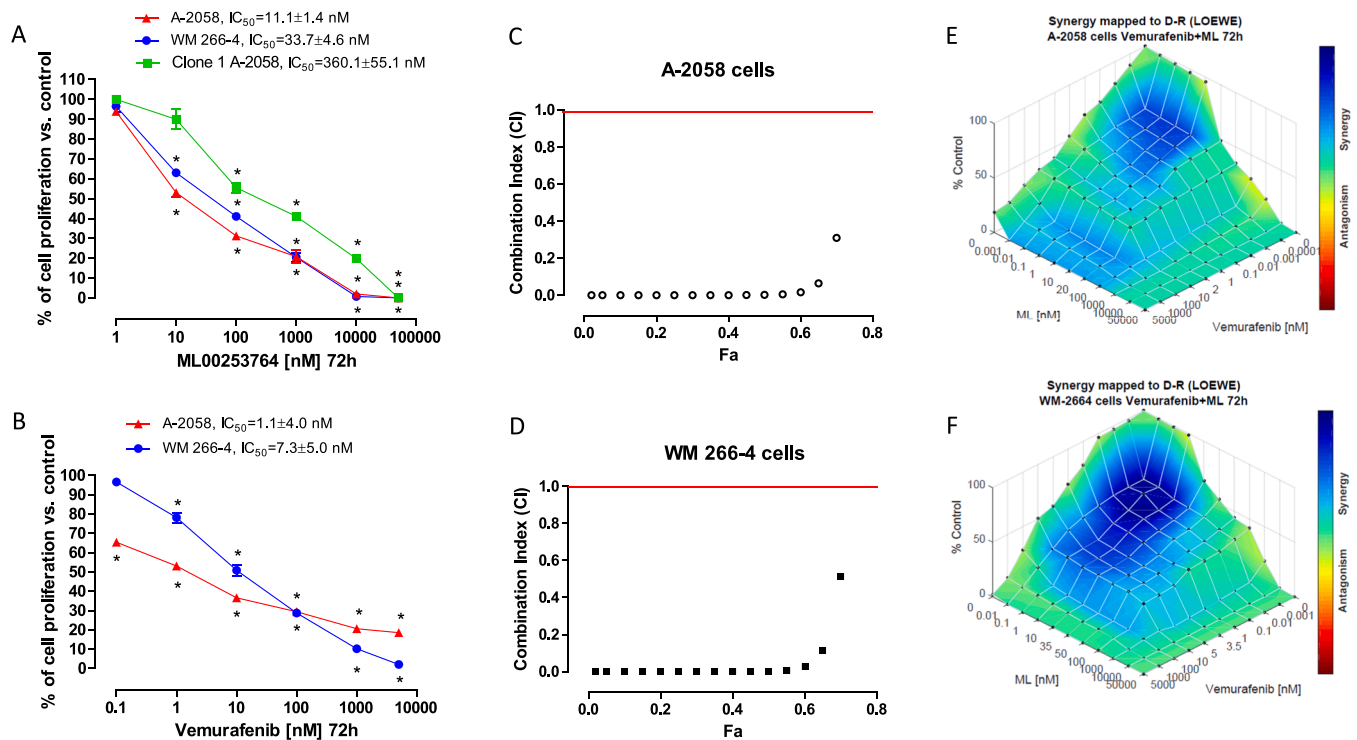


Fig. 4. Antiproliferative effect of ML00253764 (ML) *in vitro* on human A-2058, WM 266–4 and A-2058 Clone 1 melanoma cell lines (A). Antiproliferative effect of vemurafenib *in vitro* on human A-2058 and WM 266–4 (B). The antiproliferative effects of the drug were studied after 72 h of exposure. The data are presented as mean (\pm SD) percentage values of vehicle-treated cell proliferation. * $P < 0.05$ vs. controls. Combination Index (CI)/Fraction affected (Fa) curves of A-2058 (C), and WM 266–4 (D) cell proliferation inhibition by concomitant combination of ML and vemurafenib for 72 h. The symbols represent the combination index values (synergism $CI < 1$) per the fraction of cells affected by the combination. The 3-dimensional landscape of the dose matrix of combination responses for ML and vemurafenib based on the Loewe model in A-2058 (E) and WM 266–4 (F) cells, where blue reflects evidence of synergy and red represents evidence of antagonism. Cell viability was plotted as % control. (For interpretation of the references to color in this figure legend, the reader is referred to the web version of this article.)

nM of ML concentration, the quantity of BCL-XL, a critical antiapoptotic protein, was significantly declined after 72 h (Fig. 6D) in A-2058 cells, whereas other anti-apoptotic proteins such as HO-1 and pSTAT-Ser were found slightly reduced but not at a significant level (Fig. 6D) compared to vehicle-treated cells.

3.5. ML and vemurafenib concomitant combination inhibited melanoma *in vivo*

A-2058 and WM 266–4 cells injected s.c. in Athymic Nude-Foxn1tm mice expanded fast, and tumor volumes became measurable usually within 5 days after cell injections. The xenografts in vehicle-treated animals displayed a continuing augmentation in their dimensions and an exponential growth. In a first experiment, ML was able to statistically inhibit the A-2058 tumor growth (Fig. 7A), if compared to vehicle-treated mice, already after 5 days of treatment without any sign of weight loss suffered by mice (Fig. 7B). The concomitant combination of ML and vemurafenib was able to significantly slow down the A-2058 tumor growth if compared to controls (Fig. 7C), maintaining a good tolerability (Fig. 7D). The same antineoplastic activity was replicated in the WM 266–4 tumor masses (Fig. 7E) with significant differences in mean tumor volumes between the combination group and the control one. The therapeutic schedules were very beneficial and tolerable with low deficit of weight all over the time of treatment (Fig. 7F). Table 1 reports the assessment of necrosis, mitotic, apoptotic indexes and microvascular density of vehicle-treated and drug-treated A-2058 and WM 266–4 tumors. A significant decline in mitotic index was reported at both the active concomitant treatments, as well as a statistical increase

in activated caspase 3 staining in all treated samples. The microvascular count was significantly decreased in subcutaneous WM 266–4 tumors treated with ML plus vemurafenib, whereas in A-2058 this decrease did not reach the statistical threshold. In tissue samples of A-2058 melanoma from mice, a strong MC4R immunoreactivity (green color; Fig. 7G) and a faint MC1R immunostaining (red color; Fig. 7H) was demonstrated in vehicle-treated mice. The immunofluorescence of melanoma tissues incubated with both MC4R and MC1R antibody reported only few cells positive for the MC4R after the two-week treatment with ML (Fig. 7I) and an almost complete disappearance for MC4R signal in the combination group of tumors (Fig. 7J).

3.6. ML did not cause primary DNA damage and structural mutations *in vitro* and *in vivo*

ML exposure did not cause genotoxicity in terms of primary DNA damage at all concentrations used in WM 266–4, A-2058, and A-2058 Clone 1, unlike exposure to the positive control, which caused a significant induction of genotoxicity (Fig. 8A). With regard to structural mutations (chromosomal aberrations), such as NPBs, no significant increase was observed in any of the cell lines studied (Fig. 8B), except for mitomycin C-treated cells. The degree of DNA damage was evaluated by Comet assay at three different pH of electrophoretic run, in blood and tumor tissues of vehicle-treated and ML-treated groups of mice after 21 days of exposure. The results showed no genotoxicity with respect to single (pH 12.1) and double-strand breaks (pH 8) and alkali-labile sites (pH > 13), in peripheral blood cells and in cells obtained from explanted tumor tissue (Fig. 8C).

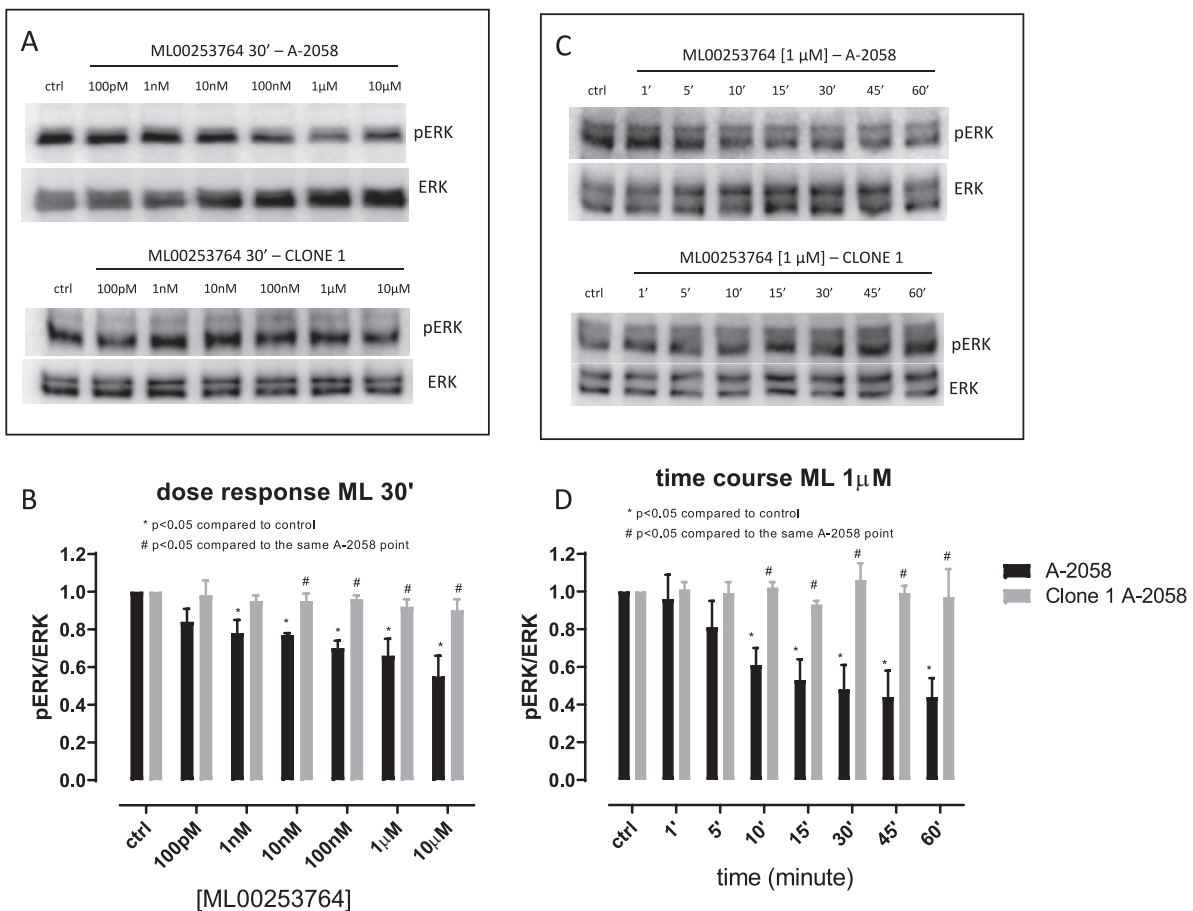


Fig. 5. (A) Immunoblotting of phospho-ERK1/2 (pERK) and total ERK1/2 (ERK) in A-2058 and A-2058 Clone 1 cell lines exposed for 30 min to 100 pM-10 μ M concentrations of ML00253764 (ML). The blot is representative of experiments repeated three times. (B) Image analysis quantification of western blot bands representing the pERK/ERK ratio of A-2058 and A-2058 Clone 1 cell lines exposed for 30 min to 100 pM-10 μ M concentrations of ML. Columns and bars, mean values \pm SD, respectively. * P < 0.05 compared to control; # P < 0.05 compared to the same A-2058 point. (C) Immunoblotting of phospho-ERK1/2 (pERK) and total ERK1/2 (ERK) in A-2058 and A-2058 Clone 1 cell lines exposed from 1 to 60 min to 1 μ M of ML. The blot is representative of experiments repeated three times. (D) Image analysis quantification of western blot bands representing the pERK/ERK ratio of A-2058 and A-2058 Clone 1 cell lines exposed from 1 to 60 min to 1 μ M of ML. Columns and bars, mean values \pm SD, respectively. * P < 0.05 compared to control; # P < 0.05 compared to the same A-2058 point.

4. Discussion

Currently, there are no published data on the expression and activity of MC4R in human cancers other than GB [11], and therefore there are no data on its modulation by selective antagonists in melanoma. This lack of information opens entirely new and unexplored fields of research on tumors that arise from cells that normally express functional MC4Rs, such as human skin melanocytes [23].

There are no comparable data about antiproliferative and proapoptotic effects of MC4R antagonists in melanoma. Nonetheless, the use of ML to inhibit MC4R blocks cell proliferation and enhances apoptotic process in glioblastoma cells at micromolar concentrations [11]. The activity of MC4R antagonist on both cell processes was achieved in melanoma cells at nanomolar concentrations. Moreover, our use of the *MC4R null* cell line (A-2058 Clone 1), whose proliferation rate and pERK/ERK 1/2 ratio was not statistically different from A-2058, confirmed the preferential activity of the antagonist ML on MC4R, as the antiproliferative IC_{50} of the drug was markedly increased when MC4R was expressed (10 nM compared to 360 nM, respectively). This preferential antitumor activity was conceivably due, in part, to the inhibition of ERK1/2 phosphorylation, as shown by the time- and concentration-dependent effect of ML in *MC4R wild-type* cell line A-2058, whereas in the *MC4R null* A-2058 cells, the inhibition of phosphorylation completely disappeared at all time points and at the different

concentrations tested, indicating that pharmacological antitumor activity is related, in part, to ERK1/2 phosphorylation, as previously observed in GB cells [11]. Indeed, like other G protein-coupled receptors, MC4R activates MAPK signaling pathways, particularly ERK1/2 pathway, in addition to activating classical G protein-mediated signaling pathways to alter secondary messenger levels [3,24]. ERK1/2 is activated by α -melanocyte-stimulating hormone (α -MSH) in mouse GT1-7 hypothalamic cells, and Chai and coworkers have shown that the MC4R antagonist SHU9119 abolished the phosphorylation of ERK1/2 in GT1-1 mouse hypothalamic cells in a concentration-dependent way [25]. However, ML could have additional and important antitumor mechanisms of action that should be investigated other than pERK inhibition, as suggested by its activity also on *MC4R null* A-2058 cell line at much higher concentrations. Future studies will help to unveil these further inhibitory patterns.

To our knowledge, there are no preclinical data of any combinations of vemurafenib and a G protein-coupled receptor antagonist with which to make an appropriate comparison. The low experimental values of vemurafenib IC_{50} s (in the nanomolar range) were obtained with a continuous exposure (daily treatments to mimic the clinical setting) of cells to vemurafenib for 72 h. The available data for WM266-4 and A-2058 that are present in literature have been generally obtained for exposures of just 24 h [26] (e.g., for WM266-4 cells) or 48 h [27,28] (e.g., for A-2058 cells), after a single treatment with resulting higher IC_{50} s.

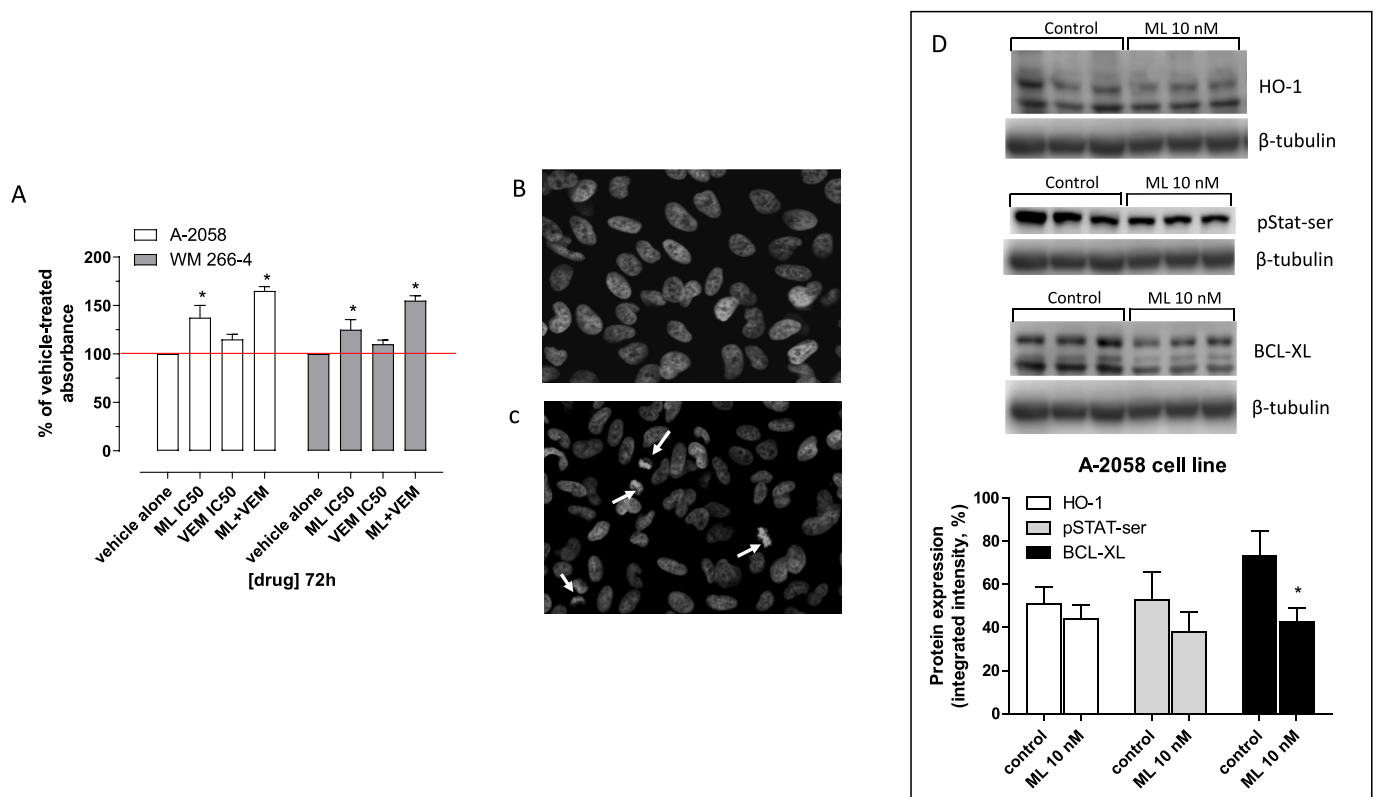


Fig. 6. Apoptosis measurements in A-2058 and WM 266-4 (A) melanoma cell lines treated with ML00253764 (ML), vemurafenib (VEM), and their simultaneous combination (at their respective IC₅₀s) using the Cell Death Detection ELISA Plus kit. The data were expressed as percentages versus the mean value of vehicle-treated absorbance (obtained from at least nine samples) that was set at 100 %. Columns and bars, mean values \pm SD, respectively. * $P < 0.05$ vs. vehicle-treated controls. A-2058 cells stained with the nuclear marker TO-PRO3 and treated with ML for 72 h. The microscopic picture shows the weak fluorescence of controls (B) with normally sized nuclei indicative of non-apoptotic cells; in the microscopic picture of cell treated with ML (C), the arrows indicate increased fluorescence of shrunken nuclei that are characteristic of apoptotic cells. Immunoblotting (D) of heme oxygenase-1 (HO-1), phospho signal transducer and activator of transcription serine (pSTAT-ser), B-cell lymphoma-extra large (BCL-XL) and of housekeeping gene product β -tubulin from a triplicate of cellular lysates of A-2058 cell line exposed for 72 h to 10 nM ML. The graph represents the image analysis quantification of western blot bands. Columns and bars, mean values \pm SD, respectively. * $P < 0.05$ compared to control.

These differences can be also ascribed to the adoption of different detection kit and procedures (e.g., MTS or MTT vs. trypan blue dye exclusion count). The enhancement of the effect of ML with a chemotherapeutic agent (e.g. temozolomide) has already been described by our group in GB cell lines both *in vitro* and *in vivo* [11], confirming the importance of a combined strategy to obtain the best antitumor results. Indeed, a synergistic effect of the combination of vemurafenib and SCH722984, an ERK1/2 inhibitor [29], on *b-raf* mutant melanoma cell lines was described, which significantly delayed the development of resistance upon long-term administration of vemurafenib [30]. Indeed, our combination treatment with ML, which was able to inhibit ERK1/2, was strongly synergistic *in vitro*, confirming this successful therapeutic approach.

Based on our previous findings in GB [11], the expected proapoptotic activity of the MC4R antagonist ML was also detected in melanoma cells at relatively much lower concentrations corresponding to the calculated antiproliferative IC₅₀s, and it was significantly enhanced by the combined treatment with vemurafenib. In addition, MC4R stimulation by α -MSH has previously been shown to provide a survival stimulus to osteoblasts by activating MC4R-sphingosine kinase 1 (SphK1) signaling [31], and to astrocytes by reducing caspase-3 activity [5]. Moreover, analogous to our results, although in a different non-neoplastic cell model, the MC4R antagonist SHU9119, and shRNA-mediated silencing of MC4R, nearly abrogated the α -MSH-induced pro-survival effect in osteoblasts [31]. In our experiments, inhibition of MC4R activity by very low concentrations of ML enhanced the apoptotic process in both melanoma cell lines by significantly reducing the anti-apoptotic protein

BCL-XL [32]. In that regard, we would argue it is not coincidental that apoptosis resistance of melanocytes is mainly related to the high expression of pro-survival mitochondrial proteins such as B-cell lymphoma 2 (BCL-2) and BCL-XL [33]. Furthermore, a recent report showed that blocking the mitochondrial protein BCL-XL increases the tendency of melanoma cells to die after therapy with various anticancer drugs, including mitotic inhibitors and chemotherapy [34]. These observations reinforce the importance of combining ML with another antineoplastic drug such as vemurafenib to enhance its antitumor effect.

The preeminent result of the *in vivo* study was that the combination of ML and vemurafenib significantly delayed subcutaneous A-2058 and WM 266-4 melanoma growth compared with either drug alone or controls, supporting the synergistic activity observed *in vitro*. Doses for either drug, which produced minimal effects when administered alone, were able to significantly reduce tumor growth and maintain the tumor response throughout the study period. Similar results were obtained when the same dose of ML 30 mg/kg was combined with temozolomide in a GB *in vivo* model [11]. Interestingly, the previously described pharmacokinetics of the drug [12] indicate that experimental inhibition of subcutaneous melanoma was achieved at drug concentrations compatible with *in vitro* antiproliferative activity. As in the *in vitro* experiments, high expression of MC4Rs was also observed in the untreated subcutaneous melanoma, a predisposing condition for response to ML and especially to the combination of vemurafenib and ML. Indeed, the MC4R was almost absent in the remaining cancer cells after treatment, suggesting a selection of clones that expressed less MC4Rs on their membranes to survive treatment. In addition, both ML and vemurafenib

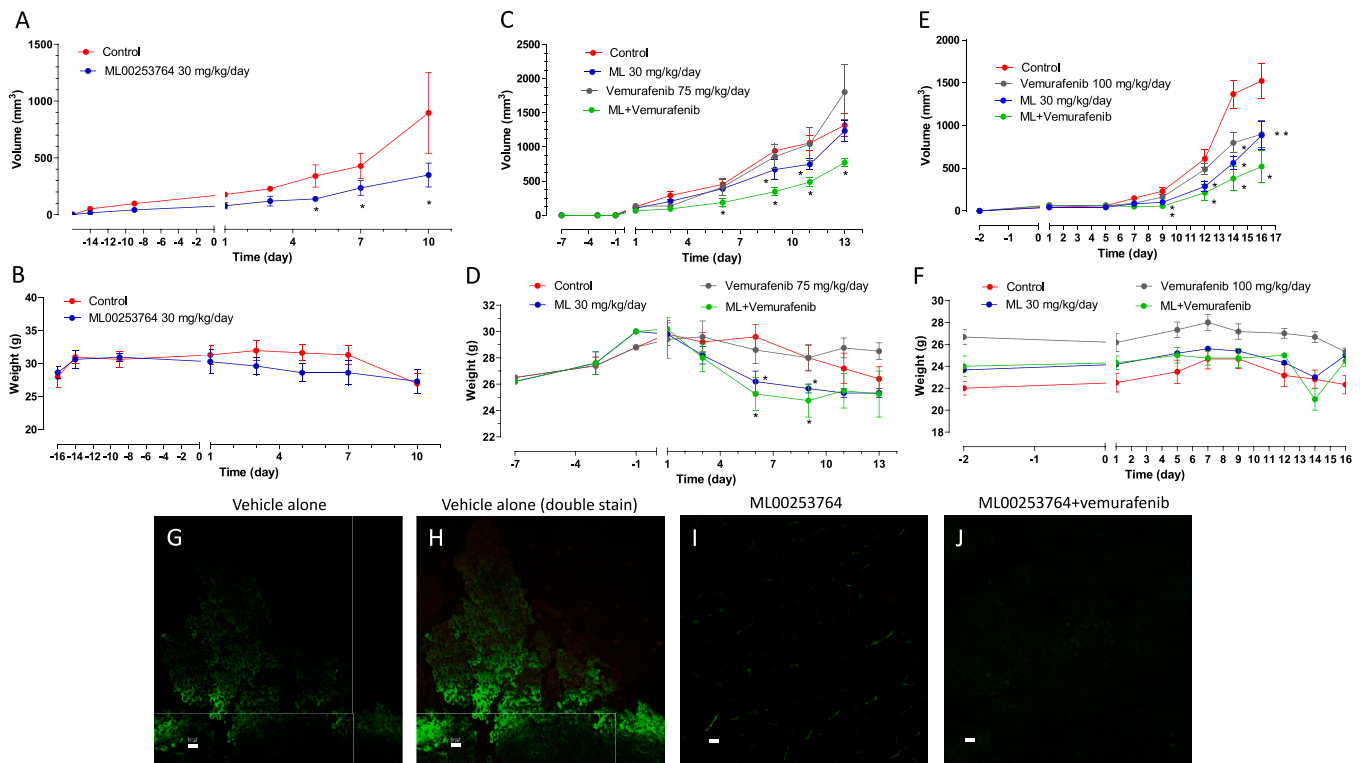


Fig. 7. In vivo therapeutic effect of (A) ML00253764 (ML) 30 mg/kg s.c. every day alone on A-2058 melanoma xenotransplant, (C) of ML concomitant combination with vemurafenib 75 mg/kg/day on A-2058 melanoma xenotransplant, and (E) of ML concomitant combination with vemurafenib 100 mg/kg/day on WM 266–4 melanoma xenotransplant in CD *nu/nu* mice. Body weight of A-2058 (B and D) and WM 266–4 (F) tumor-bearing control mice and mice treated with ML and vemurafenib alone or in combination. Symbols and bars, mean ± SD; *P < 0.05 vs. controls. MC4R and MC1R immunoreactivity in tissue samples of A-2058 melanoma xenotransplant. Vehicle-treated immunofluorescence of MC4R (G; color green) alone, vehicle-treated immunofluorescence of MC4R and MC1R (H; color red), ML-treated immunofluorescence of MC4R (I), and ML + vemurafenib-treated immunofluorescence of MC4R (J). Bar, 20 μM. (For interpretation of the references to color in this figure legend, the reader is referred to the web version of this article.)

Table 1

Necrosis index, mitotic index, microvascular count and apoptotic index of human subcutaneous melanomas after treatment of vehicle alone (control), ML00253764 alone, vemurafenib alone, and their combination (ML00253764 + vemurafenib). Values are shown as mean ± SE; *P < 0.05 vs. vehicle-treated controls.

Parameters	Necrosis index (% of necrotic area)	Mitotic index	Microvascular count (CD31 +)	Apoptotic index (% of active caspase 3 stained cells)
A-2058 tumor tissue				
control	15.0 ± 3.2	13.6 ± 1.5	5.0 ± 0.9	20.0 ± 3.2
ML00253764	48.0 ± 3.7*	7.8 ± 1.1	5.0 ± 0.8	54.0 ± 5.1*
vemurafenib	46.0 ± 5.1*	8.0 ± 0.4	5.2 ± 0.4	52.0 ± 9.7*
combination	22.5 ± 6.3	5.5 ± 0.6*	3.7 ± 0.2	50.0 ± 4.1*
WM-266-4 tumor tissue				
control	26.7 ± 3.3	9.3 ± 0.5	7.8 ± 0.7	31.7 ± 6.5
ML00253764	36.7 ± 3.2*	8.0 ± 1.0	6.0 ± 0.6	56.7 ± 8.8*
vemurafenib	43.3 ± 3.3*	6.2 ± 0.8	8.0 ± 0.9	58.3 ± 3.1*
combination	12.5 ± 2.5	4.5 ± 0.5*	2.5 ± 0.5*	55.0 ± 5.0*

decreased the mitotic index in tumor tissues when administered alone, but their combination strongly enhanced this feature, confirming the *in vitro* antiproliferative results. Activated caspase-3 levels were observed

to increase significantly after both single and combined treatment, suggesting an important pro-apoptotic role of the therapy *in vivo* as well. An unexpected finding, that surely matter deserving future investigation, was related to the data about the combination of the two drugs causing lower values of necrosis index that did not significantly differ from the controls. However, a possible explanation of this experimental result could be the fact that the remaining smaller tumor masses of the group of animals treated with combined therapy were composed by drug-selected clones of cells resistant at least to ML because of the almost complete disappearance of MC4 receptor as testified by Fig. 7J. Moreover, it is also intriguing the inhibition of the microvascular counts in the combined treatment group of mice. Indeed, our previous published findings demonstrated the presence of MC4R in the endothelial cell line HUVEC [11]. It is conceivable that ML in combination with vemurafenib may also exert a sort of synergism against cycling endothelial cells that are present in tumor masses, reducing the number of tumor microvessels.

ML and its combination with vemurafenib did not show toxic effects *in vivo*. Indeed, the mice weights did not show any important decrease during the therapy administration if compared to vehicle-treated mice. These data confirmed the capacity of ML to attenuate and prevent tumor cachexia in mice, as previously shown [35,36], through the MC4R blockade. Moreover, its safety profile was also confirmed by the absence of genotoxicity *in vitro* and *in vivo*, suggesting that ML poses no genotoxic risk under clinical conditions and can be safely used for future clinical trials. Indeed, identification of genotoxic capacity is a crucial and essential process in the advancement of a pharmaceutical agent, as it is important for human safety in terms of potential induction of cancer and hereditary damage [37]. G protein-coupled receptor antagonists are not described as drugs that cause DNA damage, such as chemotherapeutic

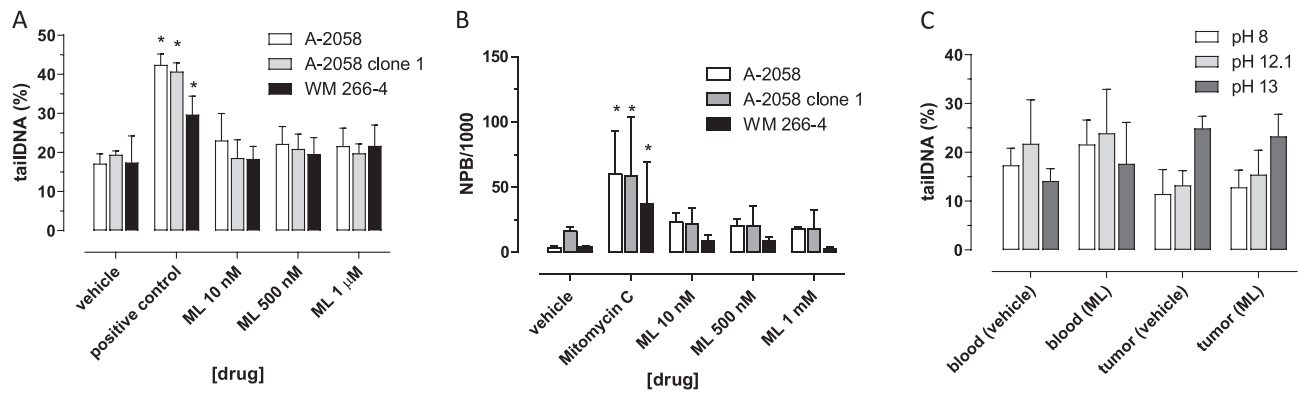


Fig. 8. (A) Levels of DNA damage in melanoma cell lines exposed to vehicle, to hydrogen peroxide (positive control) and to different concentrations of ML00253764 (ML). Results are shown as mean \pm SD. * $P < 0.05$ compared to vehicle-treated cells. (B) Frequency of nucleoplasmic bridges (NPB) in melanoma cell lines after exposure to vehicle, to mitomycin C (positive control) and to different concentrations of ML00253764 (ML). Data are shown as mean \pm SD. * $P < 0.05$ compared to vehicle-treated cells. (C) Levels of DNA damage in blood and melanoma (tumor) tissue of mice exposed to vehicle and to ML 30 mg/kg s.c. every day alone. Results are shown as mean \pm SD.

agents [38], but they require this type of investigation for their pharmacological characterization [39], in various *in vitro* and *in vivo* assays [40]. Moreover, the absence of DNA damage confirmed that the anti-melanoma activity of ML was mediated by MC4R receptor signaling inhibition as described above.

In summary, our original research and new therapeutic approaches could help change the landscape of pharmacological treatments of melanoma, adding new alternative or adjunctive drugs to established therapies.

Declaration of competing interest

The authors declare that they have no known competing financial interests or personal relationships that could have appeared to influence the work reported in this paper.

Data availability

Data will be made available on request.

Acknowledgements

The authors thank Hector Padilla of the University of Texas at El Paso for editing the English of this manuscript. Some preliminary data have been included in the international patent application PCT/IB2019/054992 of the University of Pisa and University of Modena and Reggio Emilia. The study has been funded by the “Bando Dimostratore Tecnologico” of the University of Pisa to Guido Bocci. Giulio Francia was supported by an SC1 GM136630–03 grant. Marta Banchi is supported by PNRR, Tuscany Health Ecosystem (THE), CUP 153C22000780001, and Spoke no. 7- Innovating Translational Medicine.

References

- Giuliani, A. Ottani, L. Neri, D. Zaffe, P. Grieco, J. Jochem, G.M. Cavallini, A. Catania, S. Guarini, Multiple beneficial effects of melanocortin MC4 receptor agonists in experimental neurodegenerative disorders: Therapeutic perspectives, *Prog. Neurobiol.* 148 (2017) 40–56, <https://doi.org/10.1016/j.pneurobio.2016.11.004>.
- V. Hainer, I.A. Hainerová, M. Kunesova, R.T. Braunerova, H. Zamrazilova, B. Bendlova, Melanocortin Pathways: Suppressed and Stimulated Melanocortin-4 Receptor (MC4R), *Physiol. Res.* 69 (2020) S245–S254.
- Y.X. Tao, The melanocortin-4 receptor: Physiology, pharmacology, and pathophysiology, *Endocr. Rev.* 31 (2010) 506–543, <https://doi.org/10.1210/er.2009-0037>.
- C. Caruso, L. Carniglia, D. Durand, P.V. Gonzalez, T.N. Scimonelli, M. Lasaga, Melanocortin 4 receptor activation induces brain-derived neurotrophic factor expression in rat astrocytes through cyclic AMP - Protein kinase A pathway, *Mol. Cell. Endocrinol.* 348 (2012) 47–54, <https://doi.org/10.1016/j.mce.2011.07.036>.
- C. Caruso, D. Durand, H.B. Schiöth, R. Rey, A. Seilicovich, M. Lasaga, Activation of Melanocortin 4 Receptors Reduces the Inflammatory Response and Prevents Apoptosis Induced by Lipopolysaccharide and Interferon- γ in Astrocytes, *Endocrinology*. 148 (2007) 4918–4926, <https://doi.org/10.1210/en.2007-0366>.
- S.H. Ju, G.B. Cho, J.W. Sohn, Understanding melanocortin-4 receptor control of neuronal circuits: Toward novel therapeutics for obesity syndrome, *Pharmacol. Res.* 129 (2018) 10–19, <https://doi.org/10.1016/j.phrs.2018.01.004>.
- C. Caruso, L. Carniglia, D. Durand, T.N. Scimonelli, M. Lasaga, Astrocytes: New targets of melanocortin 4 receptor actions, *J. Mol. Endocrinol.* 51 (2013) R33–R50, <https://doi.org/10.1530/JME-13-0064>.
- J.A. Benjamins, L. Nedelkoska, R.P. Lisak, Melanocortin receptor subtypes are expressed on cells in the oligodendroglial lineage and signal ACTH protection, *J. Neurosci. Res.* 96 (2018) 427–435, <https://doi.org/10.1002/jnr.24141>.
- Y.X. Tao, Constitutive activity in melanocortin-4 Receptor: Biased signaling of inverse agonists, in: *Adv. Pharmacol.*, Academic Press Inc., 2014: pp. 135–154. <https://doi.org/10.1016/B978-0-12-417197-8.00005-5>.
- W.A.J. Nijenhuis, J. Oosterom, R.A.H. Adan, AgRP(83–132) acts as an inverse agonist on the human-melanocortin-4 receptor, *Mol. Endocrinol.* 15 (2001) 164–171, <https://doi.org/10.1210/me.15.1.164>.
- F. Vaglini, C. Pardini, T. Di Desidero, P. Orlandi, F. Pasqualetti, A. Ottani, S. Pacini, D. Giuliani, S. Guarini, G. Bocci, Melanocortin Receptor-4 and Glioblastoma Cells: Effects of the Selective Antagonist ML00253764 Alone and in Combination with Temozolomide In Vitro and In Vivo, *Mol. Neurobiol.* 55 (2018) 4984–4997, <https://doi.org/10.1007/s12035-017-0702-4>.
- T.J. Vos, A. Caracoti, J.L. Che, M. Dai, C.A. Farrer, N.E. Forsyth, S.V. Drabic, R. A. Horlick, D. Lamppu, D.L. Yowe, S. Balani, P. Li, H. Zeng, I.B.J.K. Joseph, L. E. Rodriguez, M.P. Maguire, M.A. Patane, C.F. Claiborne, Identification of 2-[2-(5-Bromo-2-methoxyphenyl)-ethyl]-3-fluorophenyl]-4, 5-dihydro-1H-imidazole (ML00253764), a Small Molecule Melanocortin 4 Receptor Antagonist That Effectively Reduces Tumor-Induced Weight Loss in a Mouse Model, *J. Med. Chem.* 47 (2004) 1602–1604, <https://doi.org/10.1021/jm034244g>.
- C. Garbe, T.K. Eigentler, Vemurafenib, *Recent Results Cancer Res.* 211 (2018) 77–89, https://doi.org/10.1007/978-3-319-91442-8_6.
- T.C. Chou, Drug combination studies and their synergy quantification using the chou-talalay method, *Cancer Res.* 70 (2010) 440–446, <https://doi.org/10.1158/0008-5472.CAN-09-1947>.
- M.C. Cox, M. Banchi, S. Pelliccia, A. Di Napoli, L. Marcheselli, C. Patti, P. Anticoli Borza, R. Battistini, F. Di Gregorio, P. Orlandi, G. Bocci, All-oral metronomic DEVEC schedule in elderly patients with peripheral T cell lymphoma, *Cancer Chemother. Pharmacol.* 86 (2020) 841–846, <https://doi.org/10.1007/s00280-020-04172-3>.
- T. Di Desidero, P. Xu, S. Man, G. Bocci, R.S. Kerbel, Potent efficacy of metronomic topotecan and pazopanib combination therapy in preclinical models of primary or late stage metastatic triple-negative breast cancer, *Oncotarget.* 6 (2015) 42396–42410.
- T. Di Desidero, P. Orlandi, D. Gentile, M. Banchi, G. Ali, C. Kusmic, P. Armanetti, G. J. Cayme, L. Menichetti, G. Fontanini, G. Francia, G. Bocci, Pharmacological effects of vinorelbine in combination with lenvatinib in anaplastic thyroid cancer, *Pharmacol. Res.* 158 (2020), <https://doi.org/10.1016/j.phrs.2020.104920>.
- G. Bocci, F. Buffa, B. Canu, R. Concu, A. Fioravanti, P. Orlandi, T. Pisanu, A new biometric tool for three-dimensional subcutaneous tumor scanning in mice, *In Vivo (brooklyn)*. 28 (2014) 75–80.
- C. Atay, T. Kwak, S. Lavilla-Alonso, L. Donthireddy, A. Richards, V. Moberg, S. Pilon-Thomas, M. Schell, J.L. Messina, V.W. Rebecca, M. Xiao, J. Tan, G. Zhang, J.S. Weber, M. Herlyn, A.A. Sarnaik, D.I. Gabrilovich, BRAF targeting sensitizes resistant melanoma to cytotoxic T cells, *Clin. Cancer Res.* 25 (2019) 2783–2794, <https://doi.org/10.1158/1078-0432.CCR-18-2725>.
- V. Della Latta, M. Cabiati, S. Burchielli, G. Frenzilli, M. Bernardeschi, A. Cecchetti, F. Viglione, M.A. Morales, S. Del Ry, Lung inflammation after

- bleomycin treatment in mice: Selection of an accurate normalization strategy for gene expression analysis in an ex-vivo and in-vitro model, *Int. J. Biochem. Cell Biol.* 88 (2017) 145–154. <https://doi.org/10.1016/j.biocel.2017.05.016>.
- [21] P. Guidi, M. Nigro, M. Bernardeschi, P. Lucchesi, V. Scarcelli, G. Frenzilli, Does the crystal habit modulate the genotoxic potential of silica particles? A cytogenetic evaluation in human and murine cell lines, *Mutat. Res. - Genet. Toxicol. Environ. Mutagen.* 792 (2015) 46–52. <https://doi.org/10.1016/j.mrgentox.2015.07.005>.
- [22] P. Thomas, M. Fenech, Cytokinesis-block micronucleus cytome assay in lymphocytes, *Methods Mol. Biol.* 682 (2011) 217–234. https://doi.org/10.1007/978-1-60327-409-8_16.
- [23] J.D. Spencer, K.U. Schallreuter, Regulation of pigmentation in human epidermal melanocytes by functional high-affinity beta-melanocyte-stimulating hormone/melanocortin-4 receptor signaling, *Endocrinology.* 150 (2009) 1250–1258. <https://doi.org/10.1210/EN.2008-1212>.
- [24] E. Damm, T.R.H. Buech, T. Gudermann, A. Breit, Melanocortin-induced PKA activation inhibits AMPK activity via ERK-1/2 and LKB-1 in hypothalamic GT1-7 cells, *Mol. Endocrinol.* 26 (2012) 643–654. <https://doi.org/10.1210/me.2011-1218>.
- [25] B. Chai, J.Y. Li, W. Zhang, E. Newman, J. Ammori, M.W. Mulholland, Melanocortin-4 receptor-mediated inhibition of apoptosis in immortalized hypothalamic neurons via mitogen-activated protein kinase, *Peptides.* 27 (2006) 2846–2857. <https://doi.org/10.1016/j.peptides.2006.05.005>.
- [26] J.J. Dong, Q.S. Li, S.F. Wang, C.Y. Li, X. Zhao, H.Y. Qiu, M.Y. Zhao, H.L. Zhu, Synthesis, biological evaluation and molecular docking of novel 5-phenyl-1H-pyrazol derivatives as potential BRAFV600E inhibitors, *Org. Biomol. Chem.* 11 (2013) 6328–6337. <https://doi.org/10.1039/c3ob40776d>.
- [27] G. Yang, Y. Yan, Y. Ma, Y. Yang, Vitamin C at high concentrations induces cytotoxicity in malignant melanoma but promotes tumor growth at low concentrations, *Mol. Carcinog.* 56 (2017) 1965–1976. <https://doi.org/10.1002/mc.22654>.
- [28] H.U. Changkun, Y. Huang, L.U.O. Peixiao, Y. Yang, Effect of antioxidants coenzyme Q10 and β -carotene on the cytotoxicity of vemurafenib against human malignant melanoma, *Oncol. Lett.* 21 (2021). <https://doi.org/10.3892/OL.2021.12469>.
- [29] E.J. Morris, S. Jha, C.R. Restaino, P. Dayananth, H. Zhu, A. Cooper, D. Carr, Y. Deng, W. Jin, S. Black, B. Long, J. Liu, E. DiNunzio, W. Windsor, R. Zhang, S. Zhao, M.H. Angagaw, E.M. Pinheiro, J. Desai, L. Xiao, G. Shipp, A. Hruza, J. Wang, J. Kelly, S. Paliwal, X. Gao, B.S. Babu, L. Zhu, P. Daublain, L. Zhang, B. A. Lutterbach, M.R. Pelletier, U. Philipp, P. Siliphaivanh, D. Witter, P. Kirschmeier, W. Robert Bishop, D. Hicklin, D. Gary Gillil, L. Jayaraman, L. Zawel, S. Fawell, A.A. Samatar, Discovery of a novel ERK inhibitor with activity in models of acquired resistance to BRAF and MEK inhibitors, *Cancer Discov.* 3 (2013) 742–750. <https://doi.org/10.1158/2159-8290.CD-13-0070>.
- [30] D.J.L. Wong, L. Robert, M.S. Atefi, A. Lassen, G. Avarappatt, M. Cerniglia, E. Avramis, J. Tsoi, D. Foulad, T.G. Graeber, B. Comin-Anduix, A. Samatar, R.S. Lo, A. Ribas, Antitumor activity of the ERK inhibitor SCH722984 against BRAF mutant, NRAS mutant and wild-type melanoma, *Mol. Cancer.* 13 (2014) 194. <https://doi.org/10.1186/1476-4598-13-194>.
- [31] S. Guo, Y. Xie, J.B. Fan, F. Ji, S. Wang, H. Fei, α -Melanocyte stimulating hormone attenuates dexamethasone-induced osteoblast damages through activating melanocortin receptor 4-SphK1 signaling, *Biochem. Biophys. Res. Commun.* 469 (2016) 281–287. <https://doi.org/10.1016/j.bbrc.2015.11.104>.
- [32] L.S.W. Loo, A.A.P. Soetedjo, H.H. Lau, N.H.J. Ng, S. Ghosh, L. Nguyen, V. G. Krishnan, H. Choi, X. Roca, S. Hoon, A.K.K. Teo, BCL-xL/BCL2L1 is a critical anti-apoptotic protein that promotes the survival of differentiating pancreatic cells from human pluripotent stem cells, *Cell Death Dis.* 11 (2020) 378. <https://doi.org/10.1038/s41419-020-2589-7>.
- [33] R.A. Anvekar, J.J. Ascioffa, D.J. Missert, J.E. Chipuk, Born to be alive: A role for the BCL-2 family in melanoma tumor cell survival, apoptosis, and treatment, *Front. Oncol.* 1 (2011) 34. <https://doi.org/10.3389/fonc.2011.00034>.
- [34] V. Bharti, R. Watkins, A. Kumar, R.L. Shattuck-Brandt, A. Mossing, A. Mitra, C. Shen, A. Tsung, A.E. Davies, W. Hanel, J.C. Reneau, C. Chung, G.M. Sizemore, A. Richmond, V.L. Weiss, A.E. Vilgelm, BCL-xL inhibition potentiates cancer therapies by redirecting the outcome of p53 activation from senescence to apoptosis, *Cell Rep.* 41 (2022), 111826. <https://doi.org/10.1016/j.celrep.2022.111826>.
- [35] S. Markison, A.C. Foster, C. Chen, G.B. Brookhart, A. Hesse, S.R.J. Hoare, B. A. Fleck, B.T. Brown, D.L. Marks, The Regulation of Feeding and Metabolic Rate and the Prevention of Murine Cancer Cachexia with a Small-Molecule Melanocortin-4 Receptor Antagonist, *Endocrinology.* 146 (2005) 2766–2773. <https://doi.org/10.1210/EN.2005-0142>.
- [36] J.R. Nicholson, G. Kohler, F. Schaerer, C. Senn, P. Weyermann, K.G. Hofbauer, Peripheral administration of a melanocortin 4-receptor inverse agonist prevents loss of lean body mass in tumor-bearing mice, *J. Pharmacol. Exp. Ther.* 317 (2006) 771–777. <https://doi.org/10.1124/jpet.105.097725>.
- [37] A. Hartwig, M. Arand, B. Epe, S. Guth, G. Jahnke, A. Lampen, H.J. Martus, B. Monien, I.M.C.M. Rietjens, S. Schmitz-Spanke, G. Schriever-Schwemmer, P. Steinberg, G. Eisenbrand, Mode of action-based risk assessment of genotoxic carcinogens, *Arch. Toxicol.* 946 (94) (2020). <https://doi.org/10.1007/S00204-020-02733-2>.
- [38] I. Struys, L. Lenaerts, B. Thienpont, F. Amant, Novel next-generation sequencing-based methodologies to characterize the mutational consequences of (prenatal) chemotherapy exposure in noncancerous tissue, *Curr. Opin. Oncol.* 33 (2021) 476–484. <https://doi.org/10.1097/CCO.0000000000000755>.
- [39] C.S. Sum, B.J. Murphy, Z. Li, T. Wang, L. Zhang, M.E. Cvijic, Pharmacological Characterization of GPCR Agonists, Antagonists, Allosteric Modulators and Biased Ligands from HTS Hits to Lead Optimization, Eli Lilly & Company and the National Center for Advancing Translational Sciences, 2019. <https://www.ncbi.nlm.nih.gov/books/NBK549462/> (accessed April 19, 2023).
- [40] A. Guzmán, C. García, A.R.F. de Henestrosa, S. Riley, M.T. Ruiz, A.P. Marín, A. Tortajada, Assessment of the genotoxic potential of the antipsychotic sigma receptor ligand E-5842, *Mutat. Res.* 605 (2006) 63–77. <https://doi.org/10.1016/J.MRGENTOX.2006.02.011>.